Marshall Plan - Research Report

Solid-State NMR of Tin-Organic Frameworks for Selective Epimerization of Monosaccharides

Valérie Toussaint

Research Stay at University of California Santa Barbara from March 1st – June 7th 2024

Supervised by

Prof. Robert Mach and Assistant Prof. Irina Delidovich, Institute of Chemical, Environmental and Bioscience Engineering, TU Wien, Vienna, Austria

and

Prof. Susannah Scott, Department of Chemical Engineering, UCSB - University of California Santa Barbara, Santa Barbara, United States.

Acknowledgment

I wish to express my gratitude for the opportunity to conduct research at UCSB Santa Barbara under the mentorship of Prof. Susannah Scott. I am deeply thankful to Prof. Scott for her guidance and unwavering support throughout this project. Her scholarly insights and contributions have greatly enriched the process of interpreting the results.

I am also grateful to the entire Scott Group for their warm hospitality and encouragement during my research tenure. A special mention goes to Samantha Ausman, Jerry Hu and Jaya Nolt, whose expertise in solid-state NMR and willingness to share their knowledge have been invaluable. I would also like to thank Nick Maciulis for his insightful discussions on synthesis methodologies. This work was also supported in part by NSF Major Research Instrumentation award, MRI-1920299, for magnetic resonance instrumentation.

I am appreciative of the financial support provided by the Marshall Plan Foundation, which made this research endeavor possible. I extend my thanks to Assistant Prof. Irina Delidovich for her essential support throughout the project and for her assistance in securing the Marshall Plan grant. I would like to extend my gratitude to Diana Tsenova from the international office at TU Wien for her assistance in applying for the Marshall Plan grant and handling organizational matters.

Abstract

Developing chemo-catalytic systems capable of selectively epimerizing aldoses at the C2 atom has been challenging compared to the well-understood aldose isomerization reaction. Consequently, there is an urgent requirement for sustainable synthesis methods for solid epimerization catalysts. In this regard, tin-organic frameworks (Sn-OF) have emerged as promising catalysts for the epimerization in aqueous environments, with high stability, low tin leaching and high selectivity for the epimerization product without the addition of a soluble co-catalyst. Systematic structural characterization of the Sn-OFs *via* ^{119}Sn CP MAS and ^{119}Sn one pulse solid-state NMR and investigation of the reaction kinetics of the epimerization of D-glucose by *in situ* solid-state NMR will provide deeper insights into this rather young class of nanoporous inorganic-organic hybrid materials. Spectroscopic analysis of Sn-OF-1 shows that the structure is composed of various tin species and changes upon reaction. After the reaction, a significant amount of SnO_2 can also be identified, which affects the reusability of the catalyst.

1. Theoretical Background and State of the Art

1.1. Rare Sugars in the US

The rare sugar market in the U.S. is experiencing significant growth, driven by increased demand for low-calorie sweeteners and healthier alternatives. The market is expected to reach approximately $1.83 billion by 2029, growing at a compound annual growth rate (CAGR) of 4% from 2023 to 2029. This growth is fueled by the rising prevalence of diabetes and obesity, as well as a broader consumer shift towards healthier food and beverage options.[1, 2]

In terms of specific rare sugars, D-psicose, also known as Allulose, is a major contributor to market growth. This sugar is gaining popularity due to its low-calorie content and beneficial health properties, such as reducing blood glucose levels. It is used extensively in the food and beverage industry as a sweetener, making it the largest segment within the rare sugars market. The application of rare sugars is not limited to sweeteners; they are also used in pharmaceuticals, dietary supplements, cosmetics, and personal care products.[1]

The U.S. holds a dominant position in the North American rare sugar market, with significant contributions from companies like DuPont de Nemours Inc., Douglas Laboratories, and Sweet Cures. The market dynamics in the U.S. are influenced by factors such as advancements in production technologies, increased health awareness among consumers, and the availability of products through efficient distribution channels. The growing adoption of these sugars in various sectors is expected to continue driving market expansion in the coming years.[2]

1.2. The Sweet Potential of Rare Monosaccharides – Epimerization Reaction

In the past decades, sugars were primarily used in food industry to sweeten food and beverages. However, the rising demand towards biomass feedstocks, due to the finite nature of fossil fuel feedstocks as well as climate change, has changed the perception of sugars in society and industry. Of the 180 Gt of plant biomass formed annually worldwide, 75% are carbohydrates, which are in the form of cellulose, hemicellulose, starch, and sugars of all kinds which can be valorized towards valuable fine and platform chemicals used in pharmaceutical industry as well as in fuel industry.[3, 4] Especially cellulose and hemicellulose, consisting of polymers with C6-glucose units linked by β(1-4) glycosidic bonds and with heteropolymers primarily composed of C5 xylose units, are attractive as feedstocks for the production of monosaccharides.[5, 6] Lignocellulose, available from various waste streams such as agriculture, forestry and paper industry can be valorized towards valuable fine and platform chemicals used in pharmaceutical industry as well as in fuel industry.[3] It also serves as a source for a few readily available

monosaccharides whose isomerization and epimerization give rise to rare though highly demanded monosaccharides. Fig. 1 shows the formulae of lignocellulosic monosaccharides along with the structures of the corresponding C2 epimers and 2-ketoisomers.

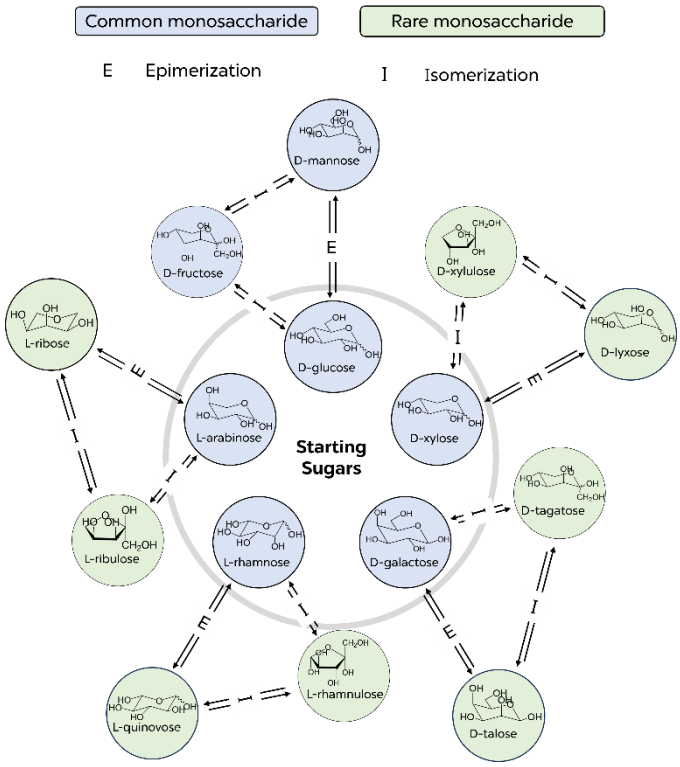

Figure 1. Summary of isomerization (I) and epimerization (E) of common sugars (blue) towards rare monosaccharides (green).

Epimerization of the common sugars D-xyl, L-ara, D-gal, and L-rham results in formation of L-lyx, L-rib, D-tal, and L-quin, respectively. Rare monosaccharides are considered as hydroxyl compounds with multiple chiral sites and are therefore considered as important raw material or ingredient in many drug and polymer syntheses and food industry.[7]

L-rib serves as a starting material for drugs targeting Hepatitis B and Epstein-Barr virus, inhibiting virus replication.[8, 9] Langenhan *et al*. found that L-rib-modified analogs of digitoxin exhibit cytotoxicity against cancer cells and tumor specificity.[9] Moreover, L-rib has a low-calorie content which makes it an attractive alternative sweetener, suitable for diabetic patients.[8] D-tal derivatives and glycoconjugates possess anti-tumor and antimicrobial properties.[10] D-Lyx, found in bacterial glycolipids, can be synthesized artificially for applications in cancer treatment.[11] L-quin, although rare and mainly found in Providencia stuartii bacteria, holds promise for pharmaceutical development.[12] Therefore, cost-effective and efficient production methods for these rare monosaccharides need to be developed.

1.3. Mechanism of the Epimerization Reaction and Suitable Catalysts

For the valorization of biomass, isomerization and epimerization are two very efficient reactions for the synthesis of rare monosaccharides on the industrial scale. The most prominent industrial-scale example is the conversion of D-glucose (D-glc) to D-fructose (D-fru).[3] Besides the isomerization of D-glc, the transformation towards its epimer D-mannose (D-man) has attracted much less attention in the past since only a few efficient chemo-catalytic systems are available for this reaction. Base-catalyzed epimerization of D-glc requires the rotation of the C2-C3 bond which makes the transformation much slower compared to the isomerization. Nevertheless, both reactions are limited by the thermodynamic equilibrium, with 55:45 glc:fru (90°C)[3, 13] isomerization, and 70:30 glc:man (90°C)[14] epimerization equilibrium ratio.

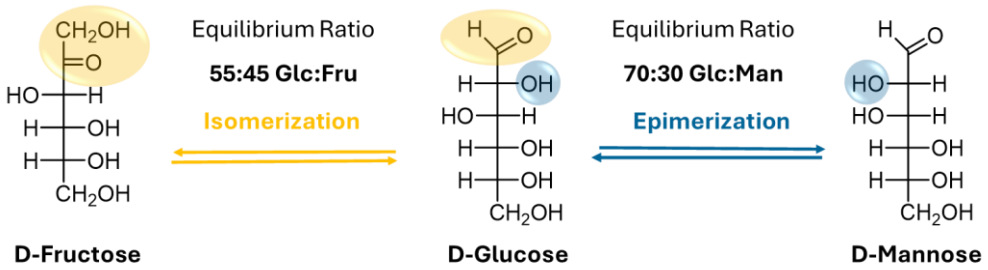

Figure 2. Isomerization of D-glc into D-fru (left) and epimerization of D-glc into D-man (right).

In industry, biocatalytic processes using epimerases are applied for the conversion of abundant sugars into rare monosaccharides. However, most epimerases are restricted to nucleotide-activated or phosphorylated sugars, excluding free monosaccharides. [10] For the production of L-rib, some large-scale productions have already been implemented such as enzymatic synthesis by isomerases. Danisco (Finland) and BioRefining (USA) succeeded in scaling up L-rib production starting from L-ara by biocatalytic transformation using D-xylose isomerase. The process is carried out in a packed bed reactor which facilitates reaction and product separation. L-Rib is isolated *via* chromatography.[9] Another approach used for the synthesis of rare monosaccharides is based on the Izumoring technique.[15] Mitsubishi Chemicals commercialized L-rib production at ton scale from D-glc, employing the Izumoring technique, involving hydrogenation, ketose formation, and enzymatic epimerization.[9, 16]

Unlike biocatalytic production methods, chemo-catalysts directly convert naturally abundant monosaccharides through epimerization into the desired product, thereby reducing the number of required reaction steps. One of the first publications describing the synthesis of rare monosaccharides with a chemo catalyst was by V. Bílik in 1972, who proposed a method for the

synthesis of D-ara from D-rib, and D-lyx from D-xyl using homogenous molybdenum containing catalysts, more specifically molybdenum oxide and molybdic acid. [17] The epimerization reaction occurs through a carbon-shift mechanism, where the monosaccharide anions coordinate to metal cations, forming a Mo(VI) dimer complex (Fig. 3). The reaction proceeds through a rearrangement of the carbon chain. This 1,2 carbon shift is known as the Bílik reaction. [18, 19]

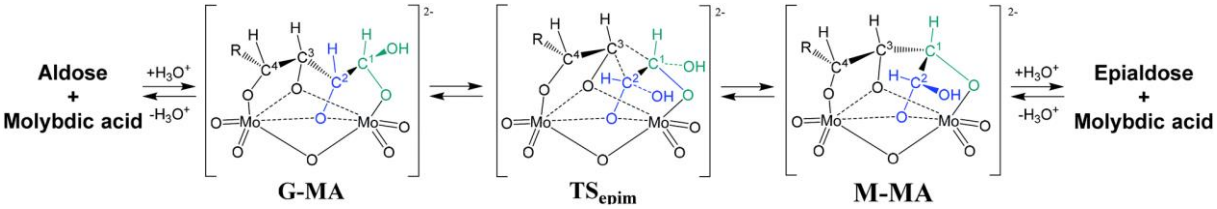

Figure 3. Accepted mechanism for the epimerization of aldose pairs, Bilik reaction, catalyzed by molybdic acid. [18, 20]

In the molybdenum acid-catalyzed epimerization reaction, the open-chain form of the aldose complexes with its four adjacent hydroxyl groups (**G-MA**) gives rise to the transient state **TS_{epim}** (Fig. 3). Breakage of the C-2-C-3 bond and the formation of the newly C1-C3 bond, results into a carbon shift of C1 and C2 and formation of a molybdate complex with the epimeric aldose (**M-MA**) (Fig. 3).[18, 20]

Furthermore, solid molybdate catalysts, such as ion exchange resins supported molybdate catalysts, were explored, which showed deactivation of the catalyst as a consequence of leaching of the active species into the liquid phase, resulting in the mannose yield being low.[21] Furthermore, metal ions combined with amine compounds as co-catalyst,[7] and solid Lewis acid catalysts with the addition of salts,[22] have demonstrated high selectivity towards the epimerization product. Nevertheless, extensive and expensive separation of the added salts and leached ions, make these catalysts hardly applicable for the industrial scale.

Due to the aforementioned drawbacks of epimerization catalysts, tin-organic frameworks (Fig.2) where Sn^{4+} ions are interconnected by organic linkers, are considered as promising solid catalysts, eliminating the need for soluble auxiliaries. Delidovich *et al.* have demonstrated that the Sn-OFs are highly selective towards the epimerization products for the following epimeric pairs: D-glc-D-man, L-ara-L-rib, D-xyl-D-lyx, and D-gal-D-tal.[23]

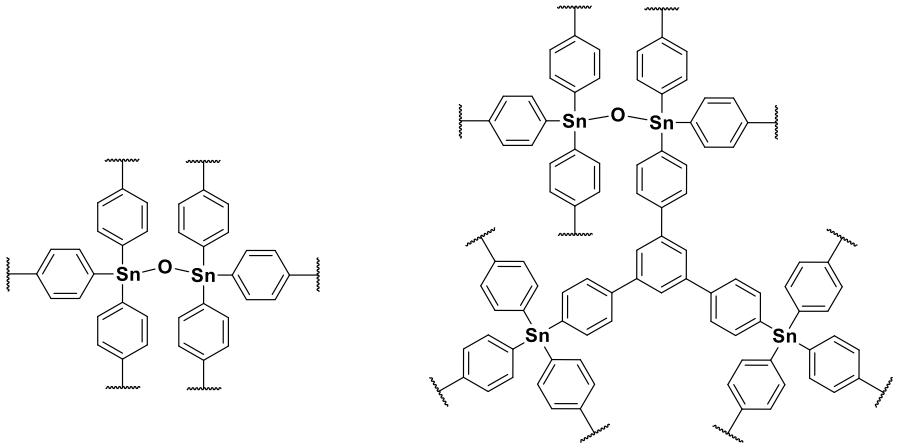

Sn-OF-1 Sn-OF-2

Figure 2. Structure of porous tin-organic frameworks synthesized by Delidovich *et al*.[23]

IR spectra of freshly synthesized Sn-OF suggest that Sn-OH groups are incorporated into the highly porous structure of the Sn-OF due to partial hydrolysis during synthesis and the work-up procedure. Nevertheless, aliphatic or Sn-O-Sn centers might also be possible catalytical centers. Sn-O-Sn centers comparable to the highly active catalytically molybdenum oxide catalysts (Fig. 3) could also catalyze the epimerization.

1.3. Solid State Nuclear Magnetic Resonance (SSNMR) and *operando* SSNMR

Solid-state nuclear magnetic resonance (NMR) is a technique used to study the structure and dynamics of solid materials at the atomic level. Solid-state NMR is employed in various fields such as materials science, pharmaceuticals, polymers, and protein structure determination. It is particularly useful for investigating complex materials like catalysts and membranes, where conventional analytical techniques may be inadequate.[24-26]

Unlike solution NMR, which deals with molecules dissolved in a liquid, solid-state NMR works directly on solid samples, offering crucial insights into materials that are insoluble, non-crystalline, or change properties upon dissolution. Key differences between solution and solid-state NMR include the absence of molecular motion in solids, which poses challenges for spectral interpretation, and the presence of anisotropic interactions such as chemical shift anisotropy, dipolar coupling, and quadrupolar coupling in solids, which affect spectral line shapes and intensities. The chemical shift anisotropy arises from the orientation dependence of the chemical shielding tensor; dipolar coupling appears due to the magnetic interaction between nuclei with non-zero magnetic moments; and quadrupolar coupling is caused by the interaction between the nuclear quadrupole moment and electric field gradients.[27]

To overcome the challenges associated with solid samples, solid-state NMR utilizes advanced techniques such as magic angle spinning (MAS), which averages out anisotropic interactions by spinning the sample at the magic angle with respect to the magnetic field; cross-polarization (CP), which enhances sensitivity by transferring polarization from abundant to less abundant nuclei; one-pulse NMR, which directly observes the nuclear magnetization without additional manipulations and offers the possibility for quantification of nuclei present within the sample.[24, 25]

Operando solid-state nuclear magnetic resonance (NMR) refers to the application of NMR spectroscopy to study chemical reactions and processes as they occur within catalytic, electrochemical, or other operating systems. This technique provides real-time insights into reaction mechanisms, intermediate species, and catalyst dynamics under realistic conditions, enabling the optimization of catalytic processes and the design of improved materials.[28, 29] *In situ* MAS NMR spectroscopy also offers the possibility for both interrogating the state of the catalytic center and identifying surface adsorbates under working conditions, thereby providing insights into kinetics and reaction mechanisms of heterogeneous catalytic reactions.[30]

2. Objective

Throughout my research, Sn-OFs demonstrated high catalytic activity and outstanding epimerization selectivity of 77-90 % for the following pairs of monosaccharides: D-glucose-D-mannose, L-ribose-L-arabinose, D-galactose-D-talose, L-rhamnose-L-quinovose, and D-xylose-D-lyxose. Furthermore, the structure of the Sn-OFs was extensively characterized by various spectroscopic methods, including ATR-IR, SEM and AFM, EXAFS and XANES, and FTIR experiments with pyridine as a probe molecule.

Even though a thorough *ex situ* characterization was done, quantification of catalytically active sites remains challenging. Results from catalytically screening triphenyltin hydroxide and bis(triphenyl)tin oxide, suggest that Sn-OH and Sn-O-Sn groups are possible catalytically active Sn centers for the epimerization of monosaccharides.

In the following fresh and spend Sn-OF-1 are analyzed *via* ^{119}Sn single pulse and ^{1}H-^{119}Sn CP MAS solid state NMR. Single NMR spectra are fitted, and quantitative results of the different Sn environments can be obtained. In addition, ^{13}C operando solid-state NMR with labeled glucose-^{13}C-1 was conducted to elucidate the reaction mechanism of the epimerization with Sn-OF-1. Kinetic profiles were collected and fitted with a kinetic model. Besides the apparent rate constants, the activation energy could also be determined.

3. Results and Discussion

3.1. Solid-state NMR of fresh and spent catalyst

Sn-OF-1 was synthesized *via* a two-fold lithiation reaction of 4,4'-dibromobiphenyl. The synthesized material exhibits a high surface area of 444 $m^2 \cdot g^{-1}$ and consists of micro- and mesopores. The tin content is approximately 21 wt%, which is in good agreement with the theoretically calculated Sn content.

The structure of Sn-OF-1 was further analyzed using ^{1}H-^{119}Sn CP MAS NMR spectroscopy. Two spectra of Sn-OF-1 were collected with a spinning rate of 10 kHz and 16 kHz as shown in Figure 4.

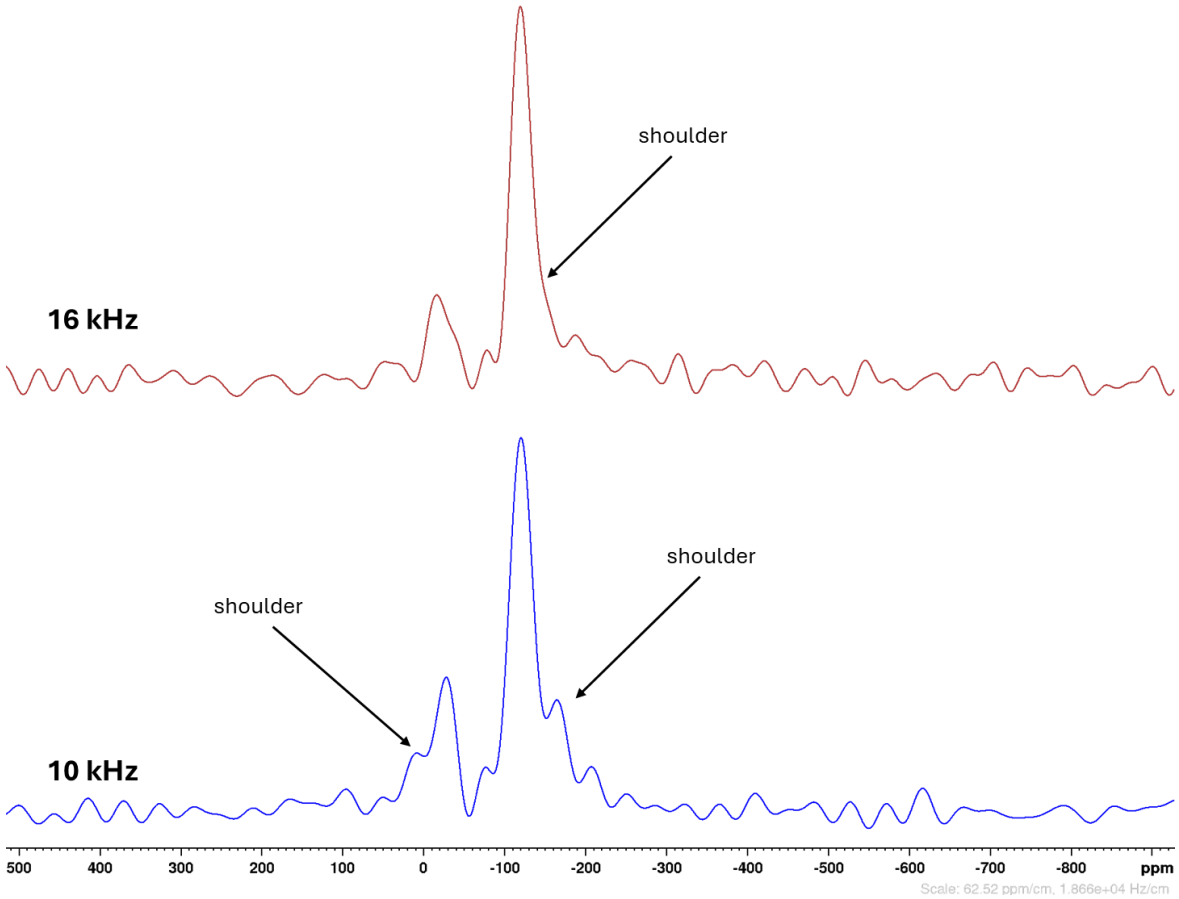

Figure 4. ^{1}H-^{119}Sn CP MAS NMR spectra of Sn-OF-1 collected at 10 kHz (bottom) and 16 kHz (top) MAS spinning rate.

The nature of the different environments can be identified by comparison of experimental and literature data with tin model substrates summarized in Fig. 24 and Table 5, respectively. The ^{119}Sn signal of the tin model substrates is influenced by the coordination number and the bonded atoms, as both change the total electron density around the tin atom. A shift to higher ppm values is caused by polar substituents and an increasing amount of aromatic linkers.

From the ^{1}H-^{119}Sn CP MAS spectra, in total, three major and two minor environments can be observed. The peak with the highest intensity and a chemical shift of -122 ppm can be assigned to tin aromatics Ph_4Sn. The environment at around -35 ppm is assigned to aliphatic chains attached to the Sn centers Bu^n_3SnPh, resulting from a side reaction with *n*-BuLi. Both environments have asymmetric peaks which suggest that there are other species integrated into the structure of the Sn-OF. The shoulder at around -14 ppm can be assigned to Bu^n_4Sn and the one at higher ppm to Ph_3-Sn-Sn-Ph_3 (-142 ppm) (Table 5, Appendix). Between these two major environments, a third environment can be identified at -78 ppm. The signal at -78 ppm in the solid-state NMR of Sn-OF-1 can be assigned to the Sn-O-Sn group as the molecular model substrate $(Ph_3Sn)_2O$ shows a similar chemical environment at -74.5 ppm, -79.8 ppm, -121 ppm (Fig. 24,

Appendix), where the latter can be assigned to an impurity of tetraphenyl tin. Comparison of both spectra at different spinning rates also shows no spinning side bands.

The structure of fresh and spent catalyst were also identified and compared by ^{119}Sn one pulse solid-state NMR. The spent catalyst for the experiment was washed with water, followed by ethanol after reaction, and dried under a high vacuum before measurement. The one pulse ^{119}Sn spectra are depicted in Figure 5. The different tin species were quantified by fitting the different environments with dmfit (Figure 9-10). The results of the fitting are summarized in Table 1.

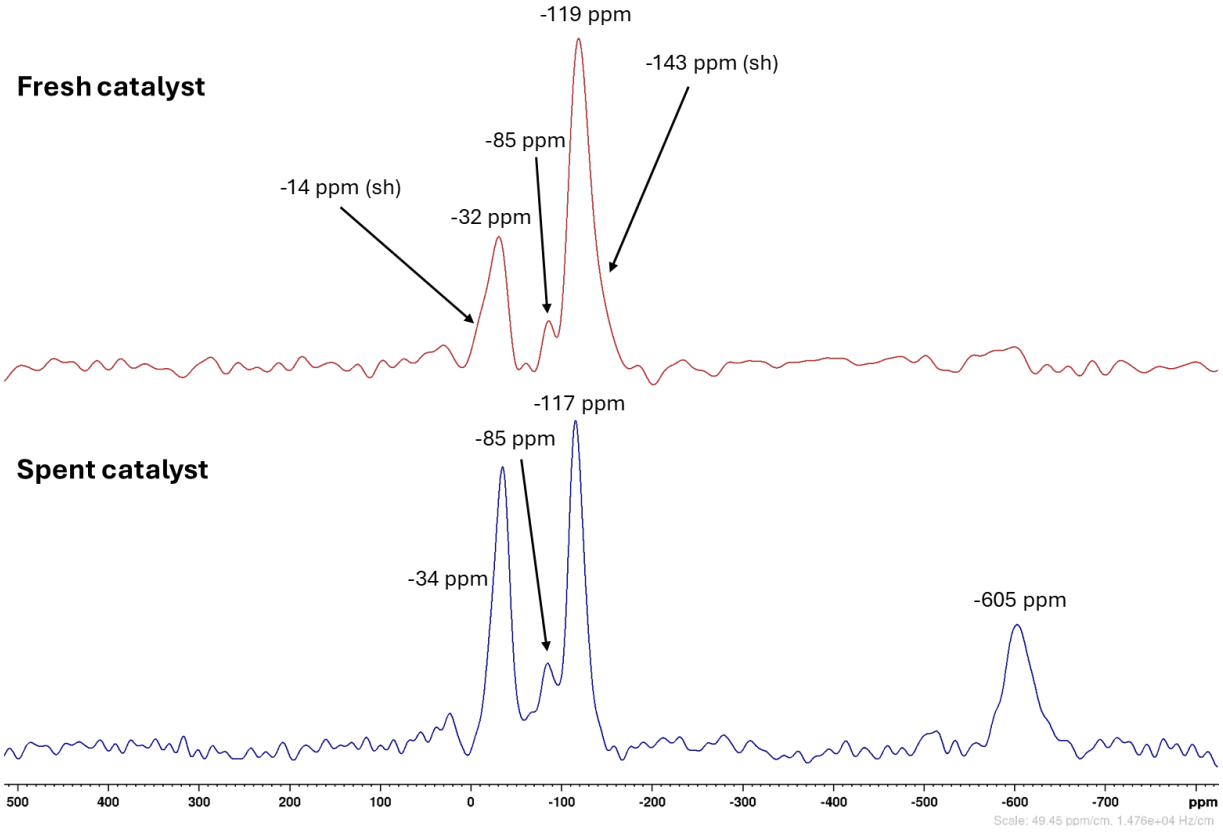

Figure 5. ^{119}Sn one pulse spectra of fresh Sn-OF-1. (800 MHz, spinning rate 28 kHz)

Table 1. Results of the fitted one pulse ^{119}Sn solid state NMR spectra.

%	Bu^n_4Sn	Bu^n_3SnPh	$(Ph_3Sn)_2O$	Ph_4Sn	$(Ph_3Sn)_2$	SnO_2
Fresh	8 (-14 ppm)	18 (-34 ppm)	4 (-85 ppm)	58 (-119 ppm)	12 (-143 ppm)	
Spent	/	32 (-32 pm)	9 (-85 ppm)	36 (-119 ppm)	/	23 (-604 ppm)

The one pulse ^{119}Sn spectrum of fresh Sn-OF-1 shows in total 5 different environments, with tin aromatic species Ph_4Sn as major environment with 58%. The spectra also shows that there are two different environments of tin aliphatic species with tin bound to 3 butyl chains or exclusively to tin chains. In addition, at -143 ppm a minor environment for a Sn-Sn bonded aromatic environment could be identified. With a chemical shift of -85 ppm, Sn-O-Sn bridges attached to aromatics substituents could be assigned, which are also suggested as main catalytically active center which react similarly to Mo centers with the open-chain form of glucose described in Section 1.2. To support this mechanism, screening of different pentoses and hexoses for the epimerization of D-glc into D-man with Sn-OF-1 showed a correlation between the number of cis-cis standing hydroxyl groups of the open-chain form of the sugars and the reaction rate for epimerization. The higher the number of cis-standing diol motifs is the higher the reaction rate.[31]

The one pulse ^{119}Sn spectra of spent catalyst shows again three major environments for Ph_4Sn (-120 ppm), $Bu^n{}_3Sn$ (-32 ppm) and $(Ph_3Sn)_2O$ (-85 ppm). The peaks for the aromatic and aliphatic Sn species are of symmetric shapes, which indicates that the minor environments for $Bu^n{}_4Sn$ and $(Ph_3Sn)_2$ were transformed. In addition, the aliphatic environment increases after the reaction, which suggests a higher amount of defects after reaction. For the spent catalyst, high amounts of SnO_2 can be observed. Tin(IV) ions can leach out by formation of strong chelate complexes with sugars in solution.[32] Consequently, SnO_2 is formed through hydrolysis of the leached tin ions, which can agglomerate on the surface and decrease the surface area of the catalyst.[33] The formation of a SnO_2-supported amorphous phase on the Sn-OF-1 surface could be responsible for the formation of fructose as a byproduct[34] and could be one of the major reasons why the selectivity and overall yield of mannose formation decreased after the recycling, as reported by Delidovich *et al*.[23]

3.2. *Operando* solid-state NMR for Epimerization of Glucose

The epimerization of D-glc into D-man takes place through carbon shift from C1 to C2. To investigate the epimerization mechanism catalyzed by Sn-OF-1, the epimerization of D-glucose-^{13}C-1 was studied at different temperatures. The reaction progress was monitored by recording a time series of direct polarization solid-state NMR spectra, shown in Figure 6, for the epimerization at 98 °C. The peaks for α- and β-glucopyranose at 92.4 ppm and 96.4 ppm, respectively, are monotonically decreasing over time. At 71.3 ppm and 71.6 ppm, signals for α- and β-mannopyranose can be observed for the formed D-mannose-^{13}C-2 due to carbon shift from C1 to C2. [23] It can also be observed that α- and β-glucopyranose have similar initial reaction rates, which suggests that glucose reacts in its open-chain form (Figure 8, Appendix). Regarding mannose formation, the reaction rate for α-mannopyranose formation is faster than for β-mannopyranose

formation (Figure 9, Appendix). The formation of α-mannopyranose might be energetically favored. Nevertheless, the ratio of β- to α-mannopyranose is constant over time (Fig.23, Appendix), suggesting that there is a fast equilibrium between these two species.

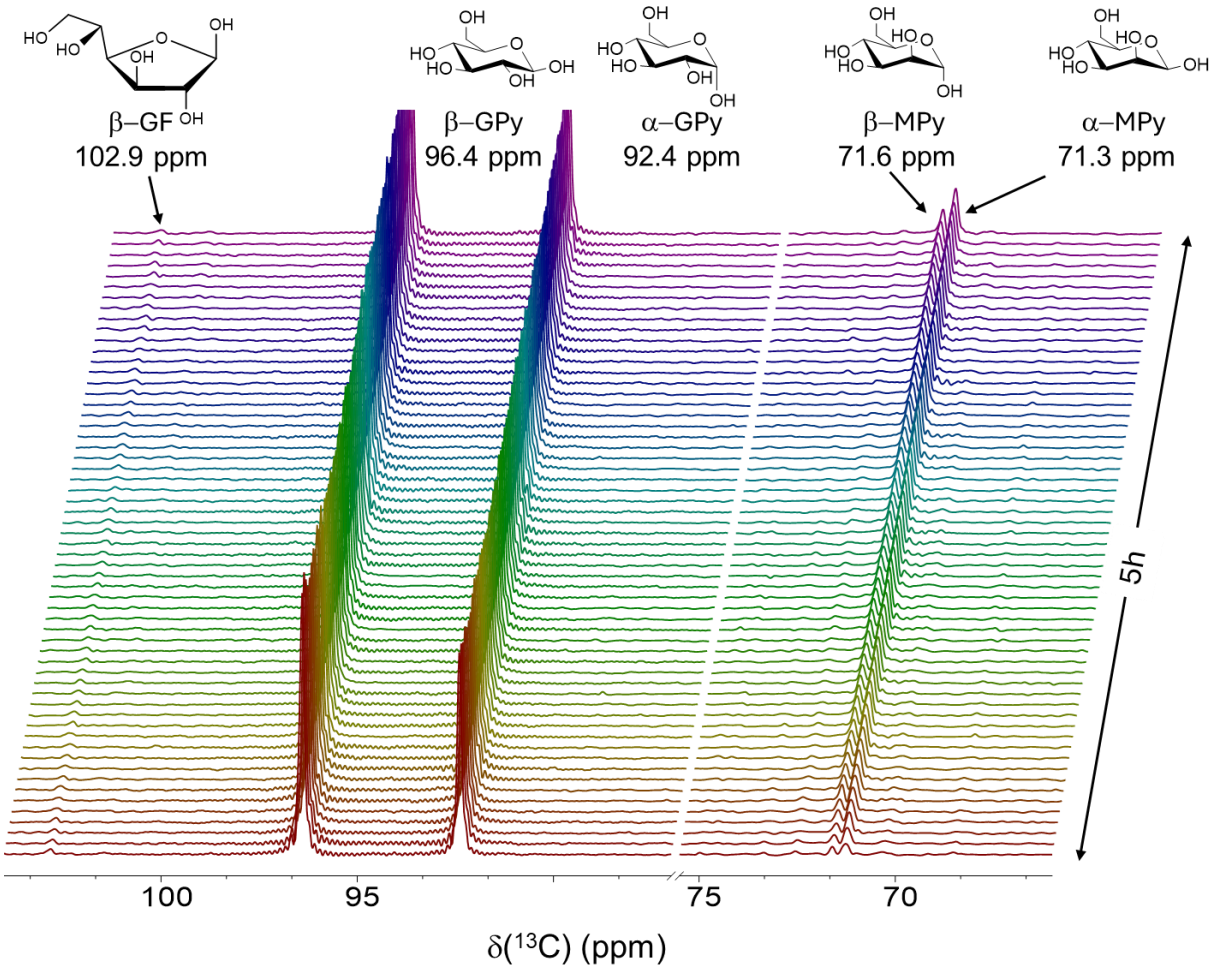

Figure 6. Direct polarization MAS solid-state ^{13}C NMR study (125.77 MHz, 3 kHz MAS) of a mixture of Sn-OF-1 (9.4 mg) with a solution of glucose-1-^{13}C (7.12 mol/L, 0.195 mL) at 92°C: time-resolved *operando* spectra showing glucose to mannose conversion.

From the NMR spectra, kinetic profiles were extracted from the total integrated area of each set of carbohydrate signals as a function of time (Fig. 15-18, Appendix). Based on the collected kinetic data, the reaction pathway shown in Figure 7 is proposed.

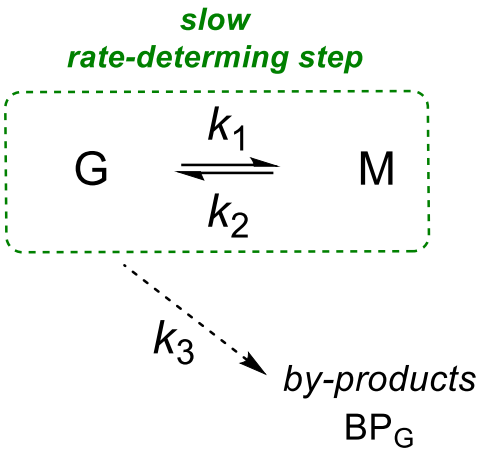

Figure 7. Proposed reaction pathway for glucose-mannose epimerization.

It is assumed that glucose epimerization to mannose is a reversible reaction with its forward and reverse reaction rate constants k_1 and k_2, respectively. In theory, one mole of glucose generates one mole of mannose *via* epimerization reaction. Nevertheless, the mass balance over time is decreasing, which suggests the formation of by-products (Fig. 20, Appendix). After the reaction, the solution also turned from colorless to light brown which indicates the formation of acidic by-products. Considering that the concentration of glucose is much higher than of mannose, herein we assume all the byproducts are formed from glucose with the reaction rate constant of k_3. Although, the formation of by-products from mannose is theoretically possible.[35] Based on this reaction pathway, the apparent kinetic equations can be described as:

$$\frac{dc_G}{dt} = -k_1 \cdot c_G + k_2 \cdot c_M - k_3 \cdot c_G \quad (1)$$

$$\frac{dc_M}{dt} = k_1 \cdot c_G - k_2 \cdot c_M \quad (2)$$

$$\frac{dc_{BP}}{dt} = k_3 \cdot c_G \quad (3)$$

By fitting the kinetic curves with equation 1 and 2 the reaction rate constants k_1, k_2, k_3 at different temperatures were obtained (Table 2) and the equilibrium constants were calculated according to the following equation:

$$\frac{k_1}{k_2} = K_{eq.} \quad (4)$$

Table 2. Rate constants and equilibrium constants for the epimerization of D-glc into D-man at different temperatures.

T [°C]	k_1 [h^{-1}]	k_2 [h^{-1}]	k_3 [h^{-1}]	$K_{eq}=k_1/k_2$
73	$8.14 \cdot 10^{-2} \pm 1.59 \cdot 10^{-2}$	$7.79 \cdot 10^{-1} \pm 2.029 \cdot 10^{-1}$	$7.30 \cdot 10^{-3} \pm 2.46 \cdot 10^{-3}$	0.10
83	$1.66 \cdot 10^{-1} \pm 2.54 \cdot 10^{-2}$	$1.19 \pm 2.17 \cdot 10^{-1}$	$2.38 \cdot 10^{-2} \pm 2.49 \cdot 10^{-3}$	0.14
88	$2.03 \cdot 10^{-1} \pm 1.53 \cdot 10^{-2}$	$1.37 \pm 1.19 \cdot 10^{-1}$	$3.29 \cdot 10^{-2} \pm 1.28 \cdot 10^{-3}$	0.15
92	$3.04 \cdot 10^{-1} \pm 3.93 \cdot 10^{-2}$	$1.80 \pm 2.58 \cdot 10^{-1}$	$3.26 \cdot 10^{-2} \pm 2.21 \cdot 10^{-3}$	0.17

Increasing the temperature shifts the equilibrium of the epimerization reaction towards mannose as indicated by an increasing equilibrium constant. In addition, the reaction constant for the formation of the side product k_3 is increasing with temperature, indicating that the production of by-products is favored at higher temperatures.

According to the Arrhenius equation:

$$\ln(k) = -\frac{\Delta E_A}{R} \cdot \frac{1}{T} + A \tag{5}$$

Where ΔE_A is the reaction activation energy, R is the gas constant and A is the pre-exponential factor. By plotting ln(k) ~ 1/T, the activation energy and the pre-factors can be determined (Figure 8) which are summarized in Table 3.

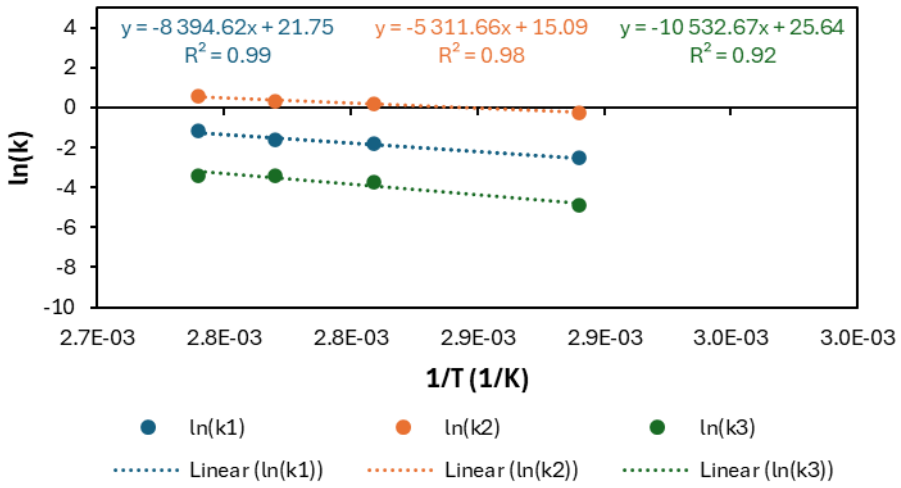

Figure 8. Arrhenius plot of the fitted data.

Table 3. Activation energy and pre-exponential factor determined by Arrhenius plot.

Entry	Reaction	ΔE_A [kJ · mol^{-1}]	A [h^{-1}]
1	Glucose→Mannose	69.8±5	21.75
2	Mannose→Glucose	44.2±5	15.09
3	Side reaction	87.6±5	25.64

Comparison of these calculated values with other apparent activation barriers reported in literature for the epimerization of glucose-mannose using other catalytic systems evidences that the $\Delta E_{A,1}$ achieved for Sn-OF-1 is lower than those reported for glucose epimerization using molybdate catalysts (**126 kJ/mol for ammonium heptamolybdate[36] and 97 kJ/mol** for molybdenum-based polyoxometalates[21]) and MOFs containing Lewis acid active sites (**88 kJ/mol for ZrMOF-808[37] and 83 kJ/mol for UiO-66(Zr)[37]).** The reverse reaction activation energy $\Delta E_{A,2}$ is 44.2 kJ/mol is significantly lower than the activation energy ΔE_1 of the forward reaction, indicating that glucose is more stable than mannose. The activation energy of the side reaction $\Delta E_{A,3}$ is 87.6 kJ/mol, which is higher than the activation energies of both forward and reverse reactions, indicating that increasing the reaction temperatures are not conducive to improving the selectivity of the target product mannose. [35]

In addition, the enthalpy of reaction ΔH can be determined by plotting the equilibrium constants (Table 2) against the reciprocals of absolute temperature according to the van't Hoff equation (Eq.5):

$$\ln(K_{\mathrm{eq.}}) = -\frac{\Delta H}{RT} + \frac{\Delta S}{R} \tag{5}$$

An enthalpy for epimerization of glucose of 25.6 kJ · mol^{-1} was calculated from the Van´t Hoff plot (Fig. 23, Appendix). A positive enthalpy indicated an endothermic reaction system, where the yield of mannose increases with increasing temperature.

4. Conclusion and Outlook

^{119}Sn Solid-state NMR of Sn-OF-1 confirms a highly porous structure composed of mainly aromatic linkers with integrated Sn sites as catalytically active centers. In addition, ^{119}Sn solid-state NMR showed that the Sn centers are not exclusively covalently bound to aromatic linkers, but due to side reactions with the butyl chain of *n*-BuLi, aliphatic chains are also attached which leads to the formation of Bu^n_3SnPh and Bu^n_4Sn sites. In addition, the structure of Sn-OF-1 changes after the reaction, as indicated by the formation of SnO_2. Also, the ratio of aromatic to aliphatic substituents changes and decreases after the reaction. A higher amount of aliphatic chains and the presence of SnO_2 could be one of the major reasons for a change in catalytic performance upon recycling reported for the Sn-OFs. A kinetic study of the epimerization of D-glucose-^{13}C-1 provides excellent insights into the reaction mechanism of Sn-OF-1. D-Man is formed *via* carbon rearrangement at C2 according to the Bilik mechanism. Interestingly, upon the reaction, the β-glucopyranose form could be observed, which is not consumed over time. Also, the activation barrier for the epimerization into man is lower than for previously reported reaction systems,

which suggests excellent catalytic performance of Sn-OF-1. As structural changes of the catalyst can be observed upon washing and drying after the reaction, the long-term stability of the catalyst should be investigated in a continuous fixed-bed reactor. The catalyst could also be further improved by grafting tin species on the surface of microspheres. Thus, the nature and the number of Sn-O groups on the surface could be controlled.

5. Experimental

5.1. Synthesis of Sn-OF-1

4,4'-Dibromobiphenyl (98%) (3.12 g, 10 mmol, 1 eq.) were dissolved in dry THF (200 mL). The solution was cooled down to -10 °C and n-BuLi (2.5 M in hexane, 8.0 mL, 20 mmol, 2 eq.) was added dropwise. The solution was stirred for 30 min and $SnCl_4$ (0.58 mL, 5 mmol, 0.5 eq.) was added dropwise. The mixture was warmed to room temperature and stirred overnight. The mixture was filtered and the obtained solid was washed twice with THF (200 mL), distilled water (200 mL) and ethanol (200 mL). The solid was dried under vacuum. Sn-OF-1 was obtained as a white powder (2.02 g, 9.57 mmol, 95.7%).

5.2. ^{1}H-^{119}Sn CP MAS and ^{119}Sn single pulse MAS Solid State NMR

^{119}Sn MAS NMR and ^{1}H-^{119}Sn CP MAS NMR experiments were carried out at a Bruker AVANCE III Ultrashield Plus 800 MHz (18.8T) with a 2.5 mm double-resonance probe. The resonance frequencies were 800.2447 MHz and 298.3868 MHz for ^{1}H and ^{119}Sn, respectively. Single-pulse excitation ^{119}Sn MAS experiments were performed on Sn-OF-1 by using a π/6 pulse and a magic angle spinning rate of 28 kHz. The ^{119}Sn chemical shift was referenced to tin chloride at −150 ppm ^{1}H-^{119}Sn CP MAS experiments were performed at a spinning rate of 10/16 kHz. The ^{119}Sn chemical shift was referenced to tetracyclohexyltin at −94.8 ppm. Each spectrum was accumulated for ca. 24 h.

5.3. Operando Solid-State ^{13}C MAS NMR Spectroscopy

The epimerization of 1-^{13}C-glucose was monitored using *operando* Magic Angle Spinning (MAS) NMR spectroscopy equipped with a 11.7 T magnet, operating at 125.7788 MHz for the ^{13}C channel and 500.2185 MHz for the ^{1}H channel. In ^{13}C direct polarization experiments, a 35 kHz ^{1}H decoupling field was employed.

In a typical experiment, 9.4 mg Sn-OF-1, 90 mg H_2O, 90 mg EtOH and 25 mg D-glucose-1-^{13}C were added to the rotor (i.d. 7.5 mm, volume 0.4 mL). After heating to the respective temperature and establishing a stable MAS rate of 3 kHz, the recording of quantitative ^{13}C MAS NMR was started. For each spectrum, 8 scans were acquired with an acquisition time of 30 ms for ^{13}C and 8 ms for

^{1}H with a spectral width of 50-5 kHz for each scan. ^{13}C chemical shifts were referenced to adamantane (38.5 ppm). Time-resolved NMR spectra were recorded with a time interval of 5 min 22 s over 5-6 h at 73, 83, 88, 92°C. The relative concentrations of D-glc and D-man were estimated by the integration of all signals. The change in the concentration of each reactive species was described as a function of time using ordinary differential equations (ODEs). The system of ODEs was fitted to the kinetic data using nonlinear least-squares regression in Python to estimate apparent rate constants at each reaction temperature.

6. Appendix

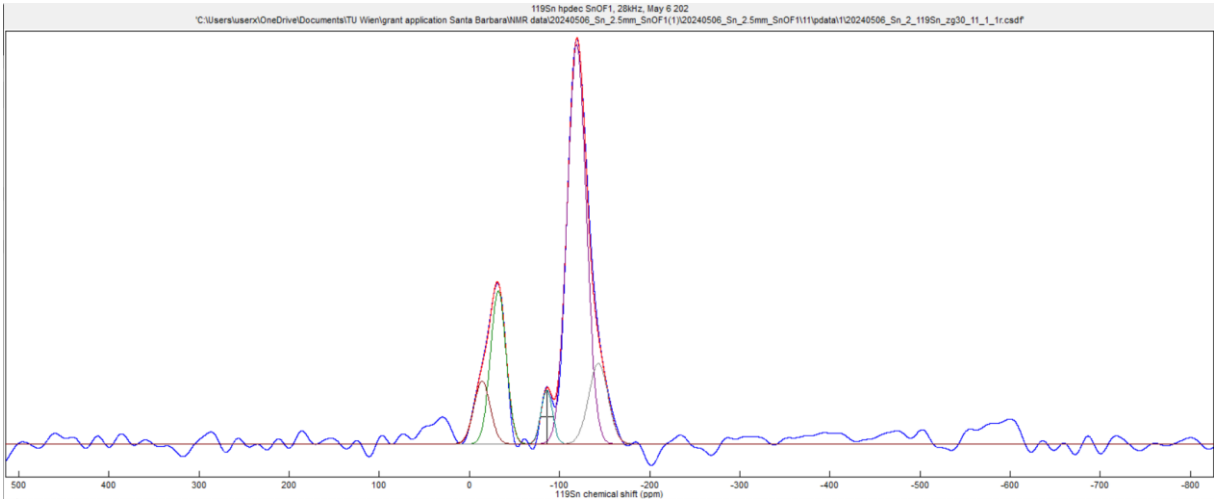

Figure 9. ^{119}Sn one pulse spectra of fresh Sn-OF-1 fitted with dmfit. The enveloping of the fitted curve is represented by the red line.

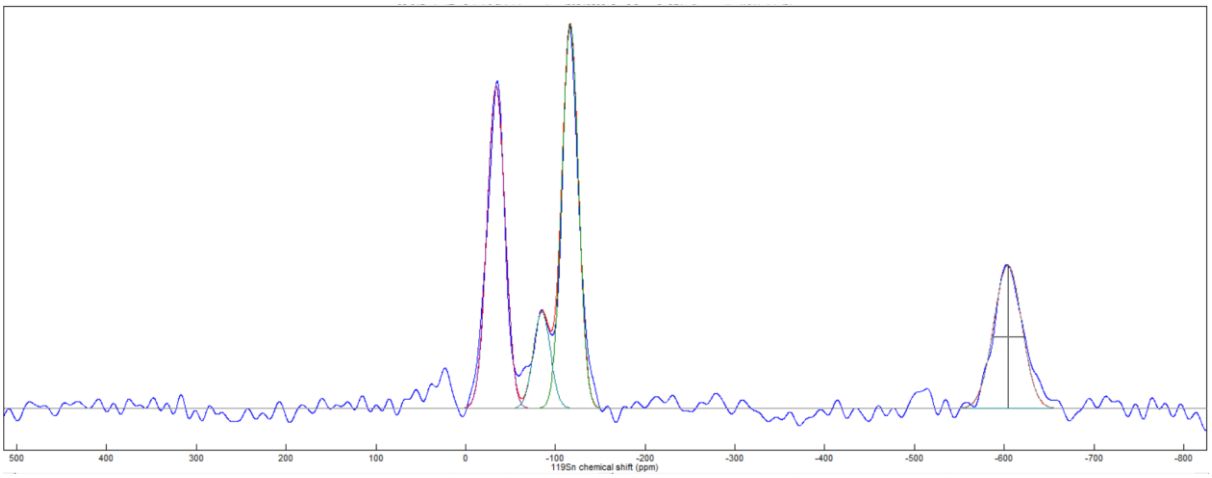

Figure 10. ^{119}Sn one pulse spectra of spent Sn-OF-1 fitted with dmfit. The enveloping of the fitted curve is represented by the red line.

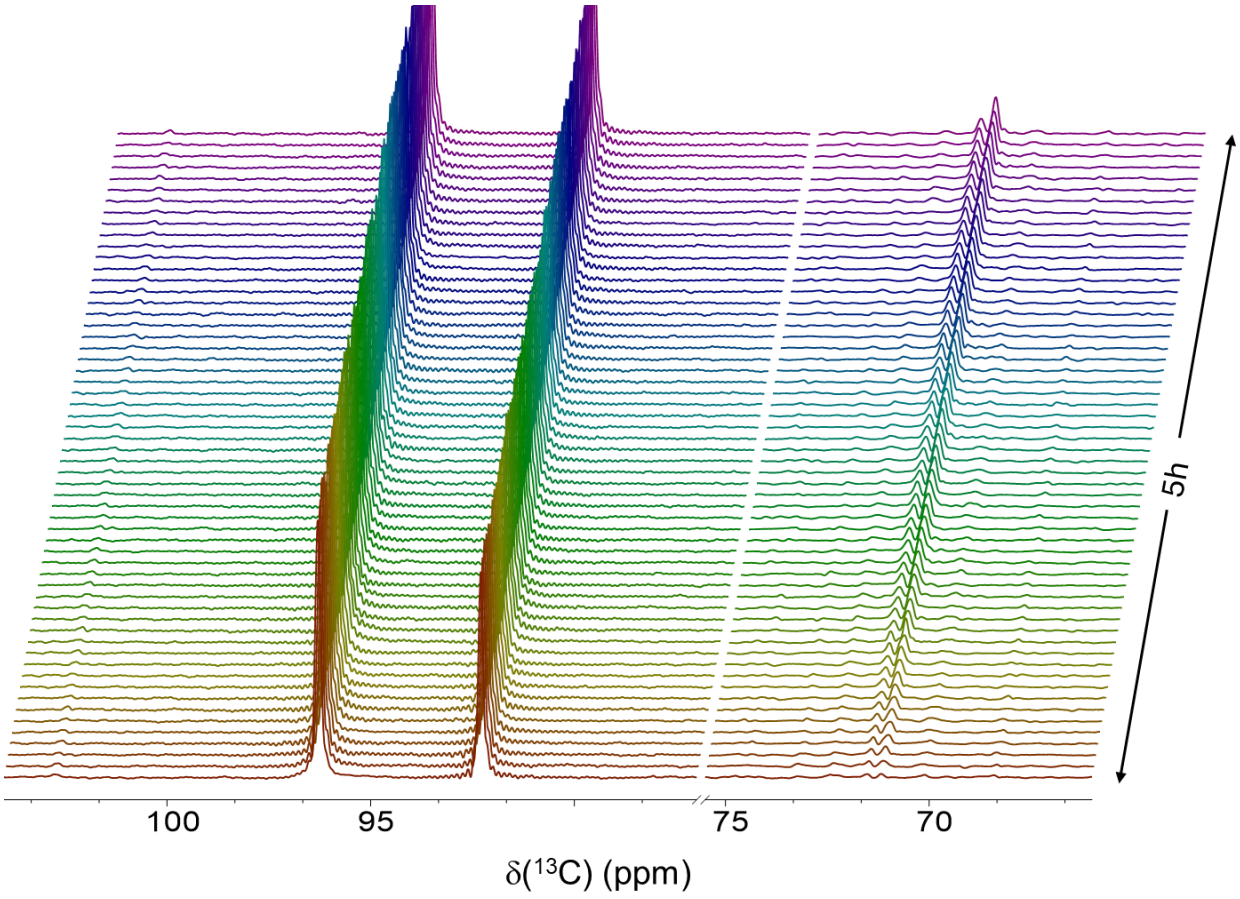

Figure 11. Direct polarization MAS solid-state ^{13}C NMR study (125.77 MHz, 3 kHz MAS) of a mixture of Sn-OF-1 (9.4 mg) with a solution of glucose-^{13}C-1 (7.12 mol/L, 0.195 mL) at **73°C**: time-resolved operando spectra showing glucose to mannose conversion.

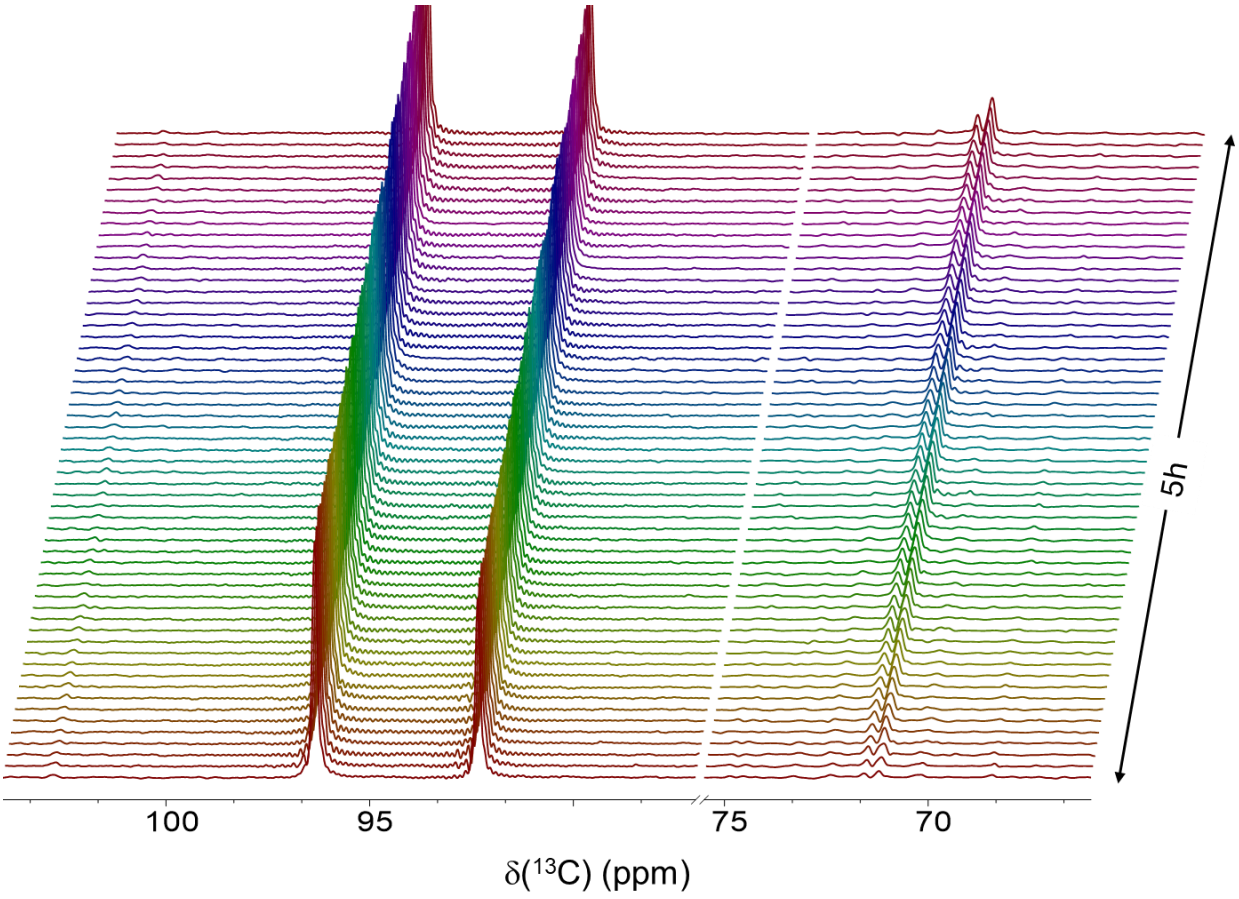

Figure 12. Direct polarization MAS solid-state ^{13}C NMR study (125.77 MHz, 3 kHz MAS) of a mixture of Sn-OF-1 (9.4 mg) with a solution of glucose-^{13}C-1 (7.12 mol/L, 0.195 mL) at **83°C**: time-resolved operando spectra showing glucose to mannose conversion.

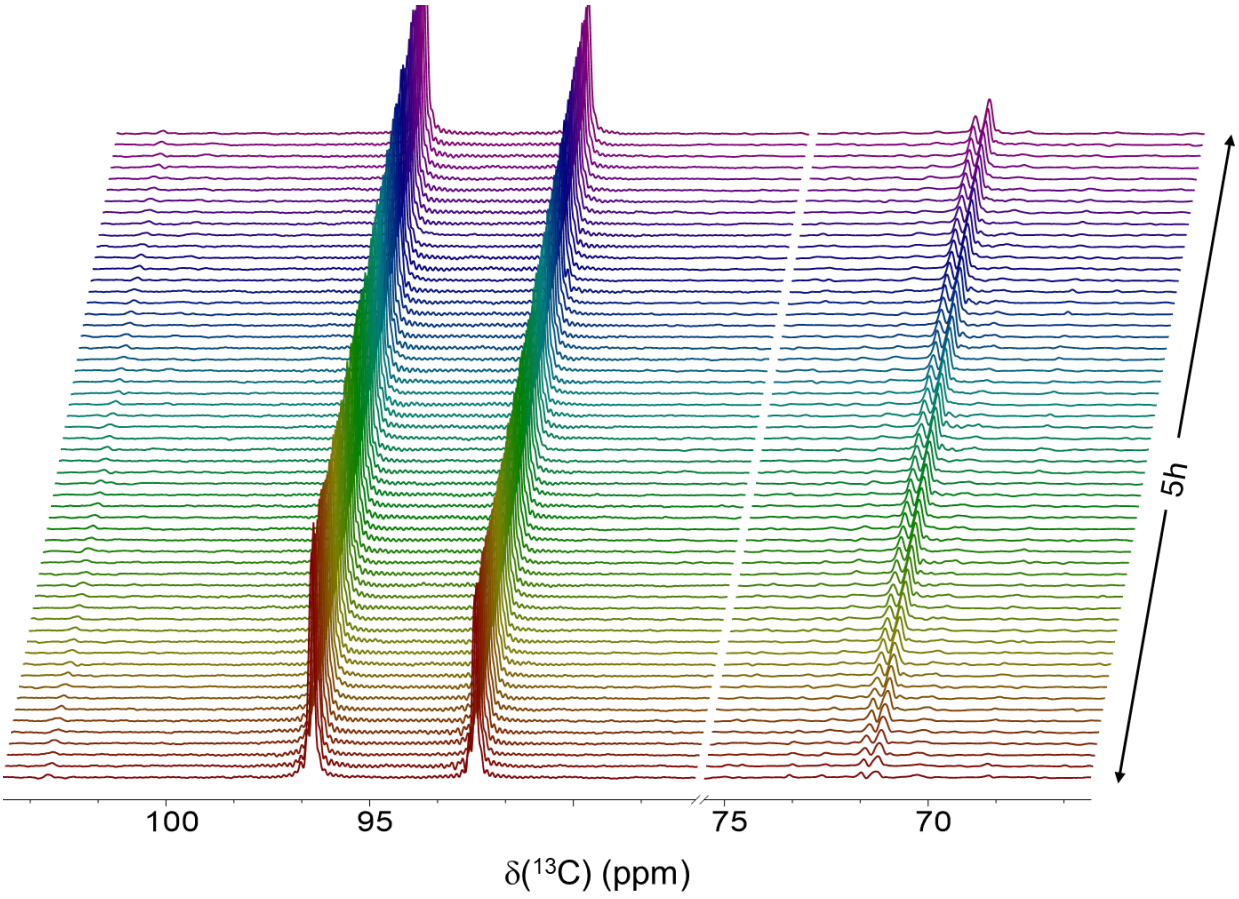

Figure 13. Direct polarization MAS solid-state ^{13}C NMR study (125.77 MHz, 3 kHz MAS) of a mixture of Sn-OF-1 (9.4 mg) with a solution of glucose-^{13}C-1 (7.12 mol/L, 0.195 mL) at **88°C**: time-resolved operando spectra showing glucose to mannose conversion.

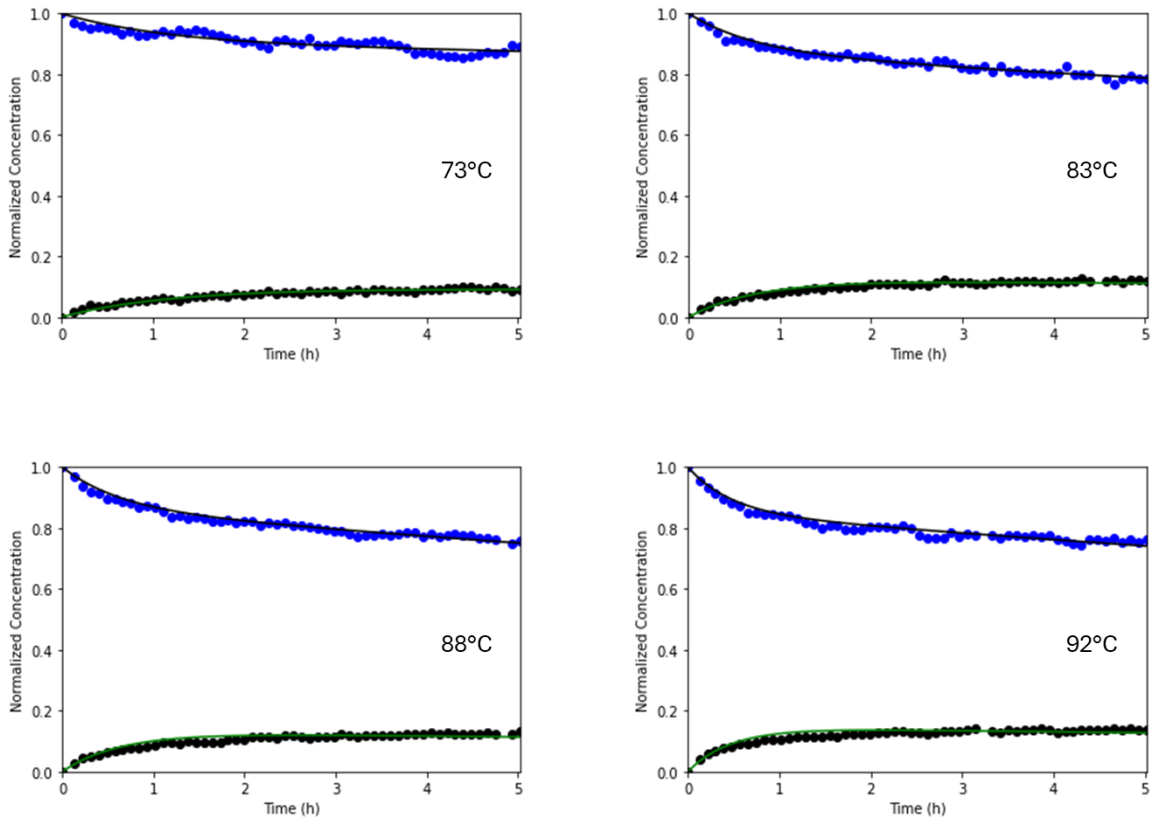

Figure 14. Fitted kinetic plots for D-glucose-^{13}C-1 epimerization at different temperatures. Reaction conditions: 25 mg D-glc-^{13}C-1, 90 mg water, 90 mg EtOH, 9.4 mg Sn-OF-1.

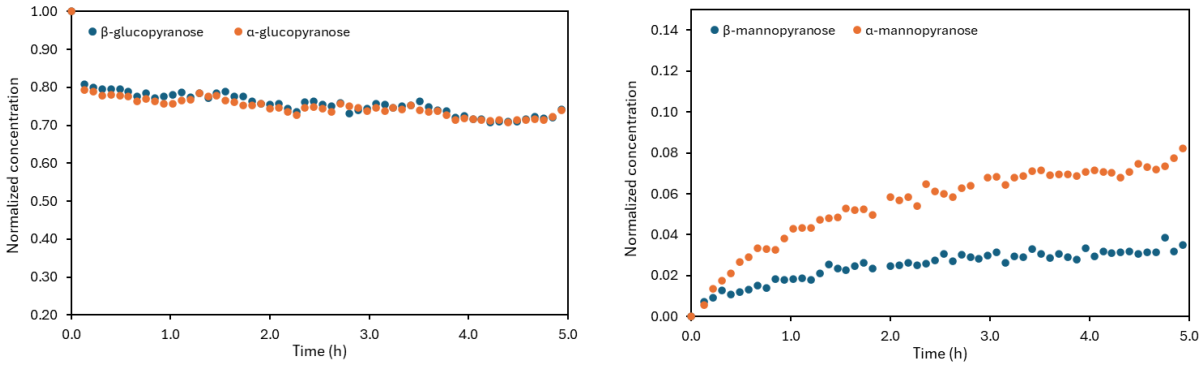

Figure 15. Time-resolved concentration curves of α–C1- and β-C1-glucopyranose (left) and α-C1- and β-C1-mannopyranose (right) at 73°C (9.4 mg Sn-OF-1 with a solution of glucose-1-^{13}C (7.12 mol/L, 0.195 mL)).

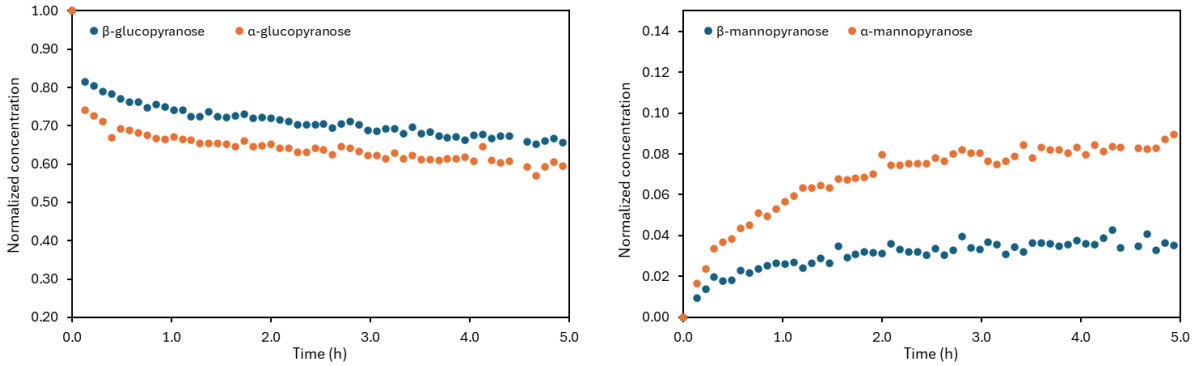

Figure 16. Time-resolved concentration curves of α–C1- and β-C1-glucopyranose (left) and α-C1- and β-C1-mannopyranose (right) at 83°C (9.4 mg Sn-OF-1 with a solution of glucose-1-^{13}C (7.12 mol/L, 0.195 mL)).

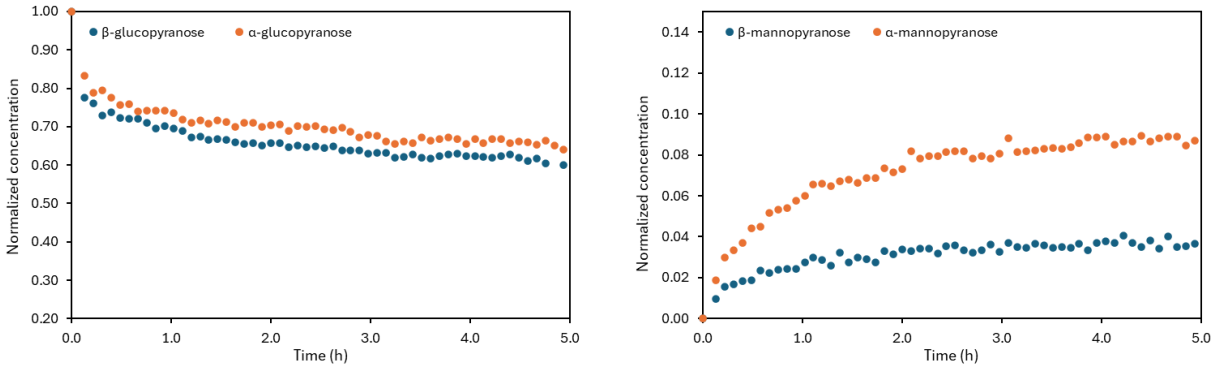

Figure 17. Time-resolved concentration curves of α–C1- and β-C1-glucopyranose (left) and α-C1- and β-C1-mannopyranose (right) at 88°C (9.4 mg Sn-OF-1 with a solution of glucose-1-^{13}C (7.12 mol/L, 0.195 mL)).

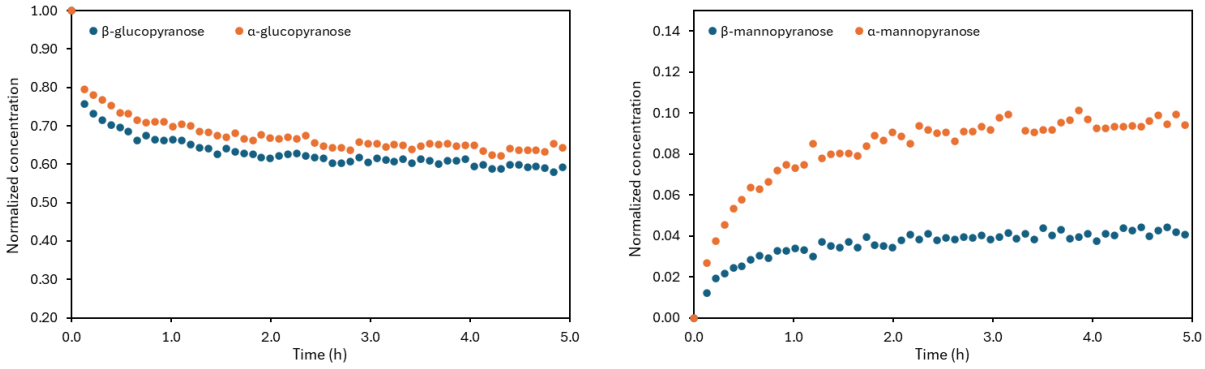

Figure 18. Time-resolved concentration curves of α–C1- and β-C1-glucopyranose (left) and α-C1- and β-C1-mannopyranose (right) at 92°C (9.4 mg Sn-OF-1 with a solution of glucose-1-^{13}C (7.12 mol/L, 0.195 mL)).

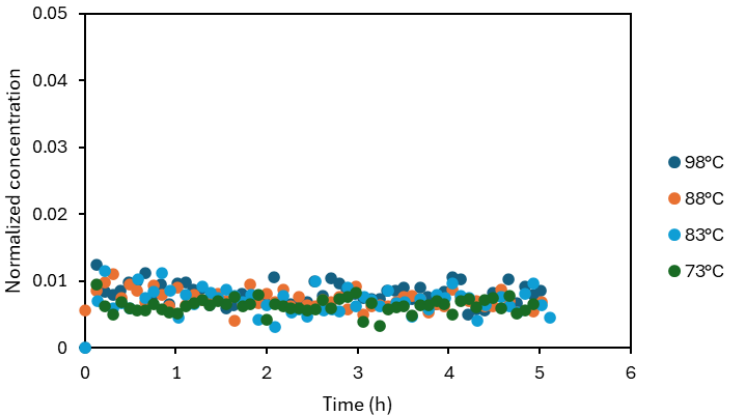

Figure 19. Concentration-time curve of β-glucofuranose at different temperatures.

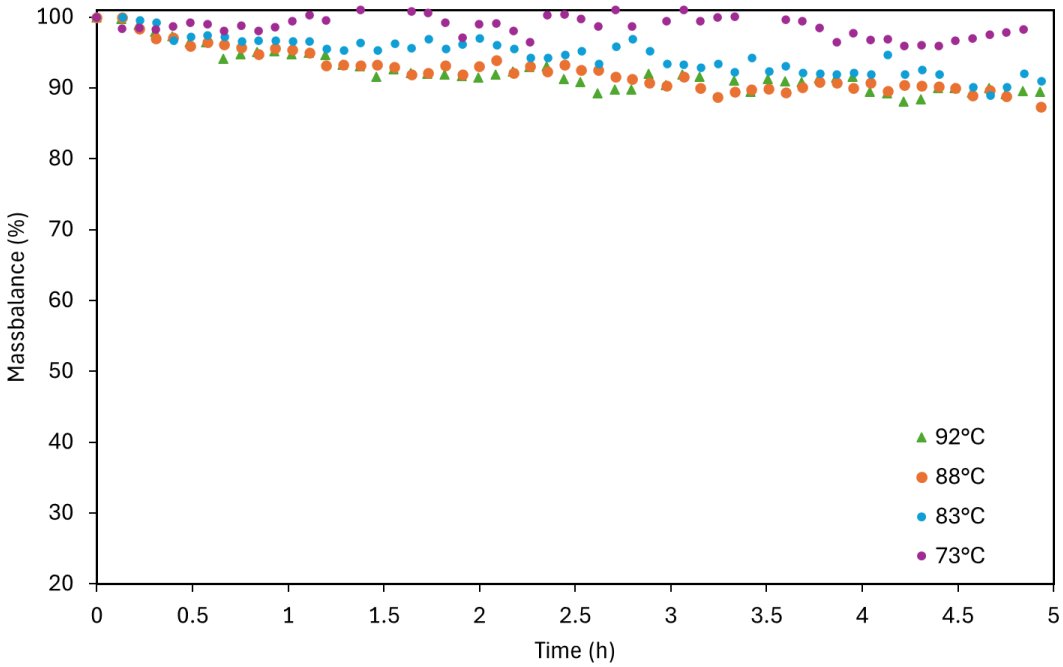

.

Figure 20. Mass balance of D-glucose-^{13}C-1 epimerization at 355 K (9.4 mg Sn-OF-1 with a solution of glucose-1-^{13}C (7.12 mol/L, 0.195 mL)).

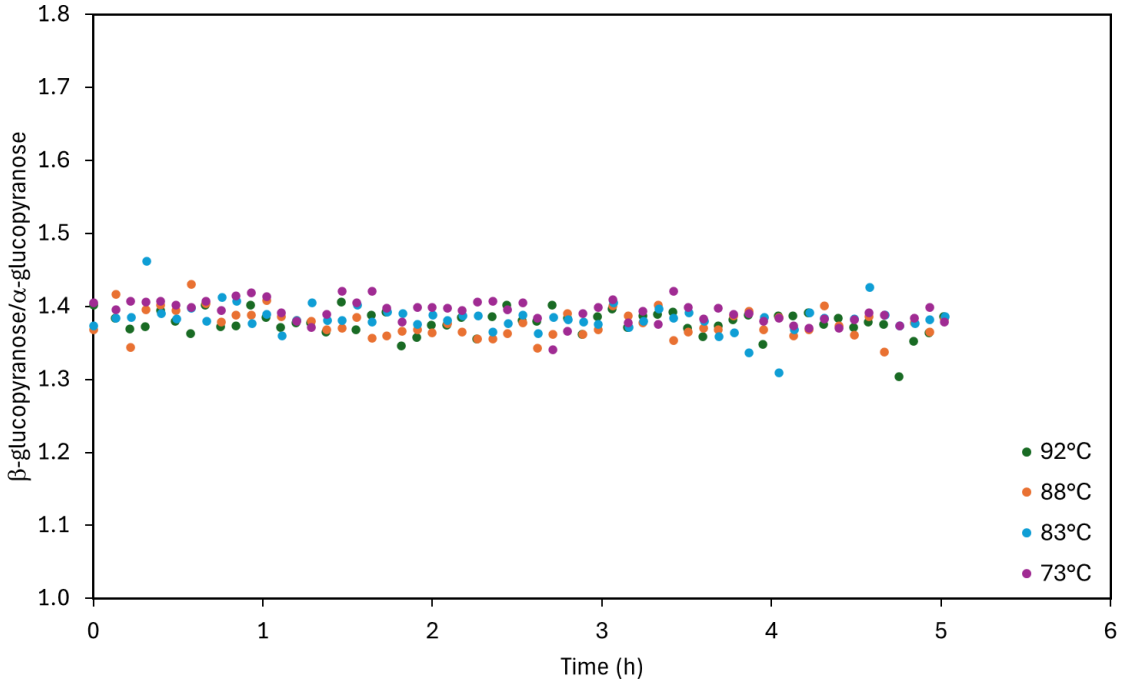

Figure 21. Ratio of β- to α-glucopyranose over time for epimerization at different temperatures.

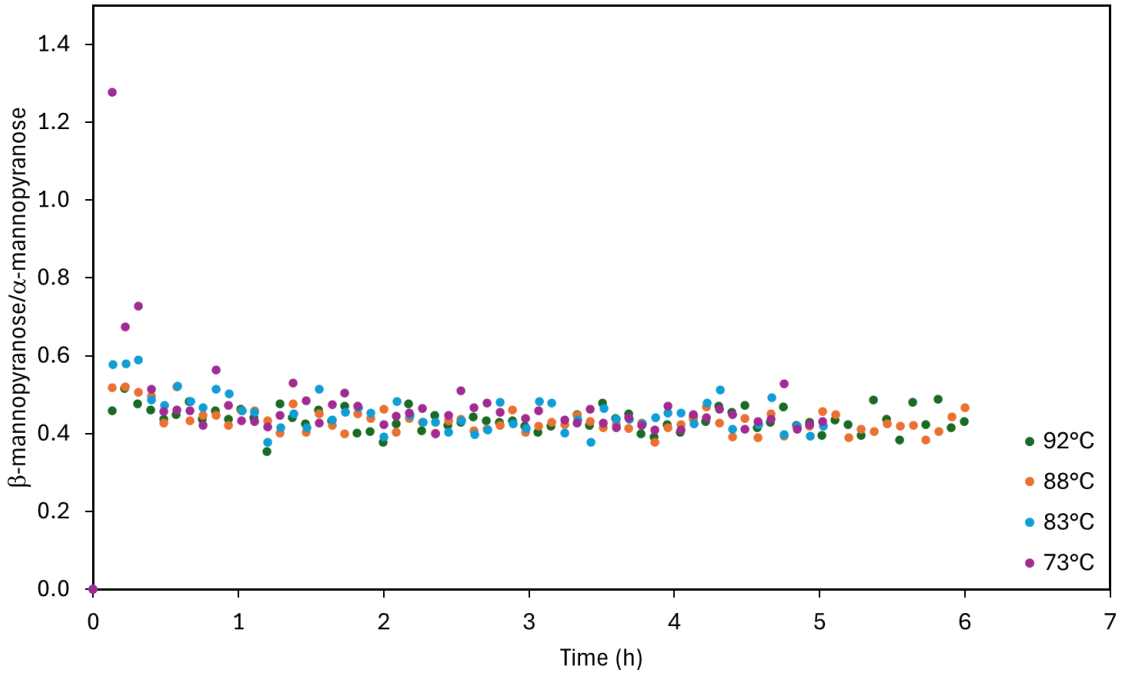

Figure 22. Ratio of β-C1- to α-C1-mannopyranose over time for epimerization at different temperatures.

Table 4. Overall ratio of α-glucopyranose, β-glucopyranose, α-C1-mannopyranose and β-C1-mannopyranose for different temperatures.

Temperature (°C)	α-GPy : β-GPy	α-MPy : β-MPy
73	58 : 42	32 : 68
83	58 : 42	31 : 69
88	58 : 42	30 : 70
82	58 : 42	30 : 70

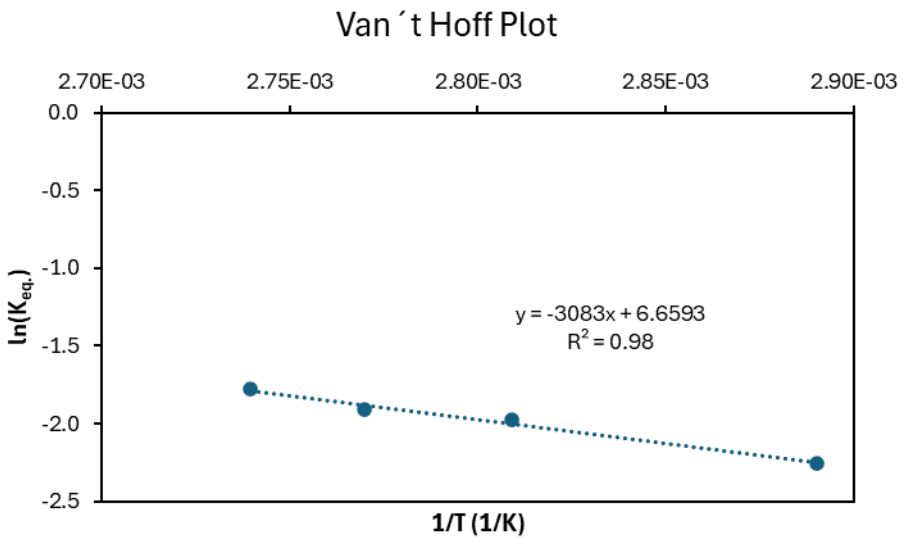

Figure 23. Van ´t Hoff plot of epimerization of D-glc into D-man.

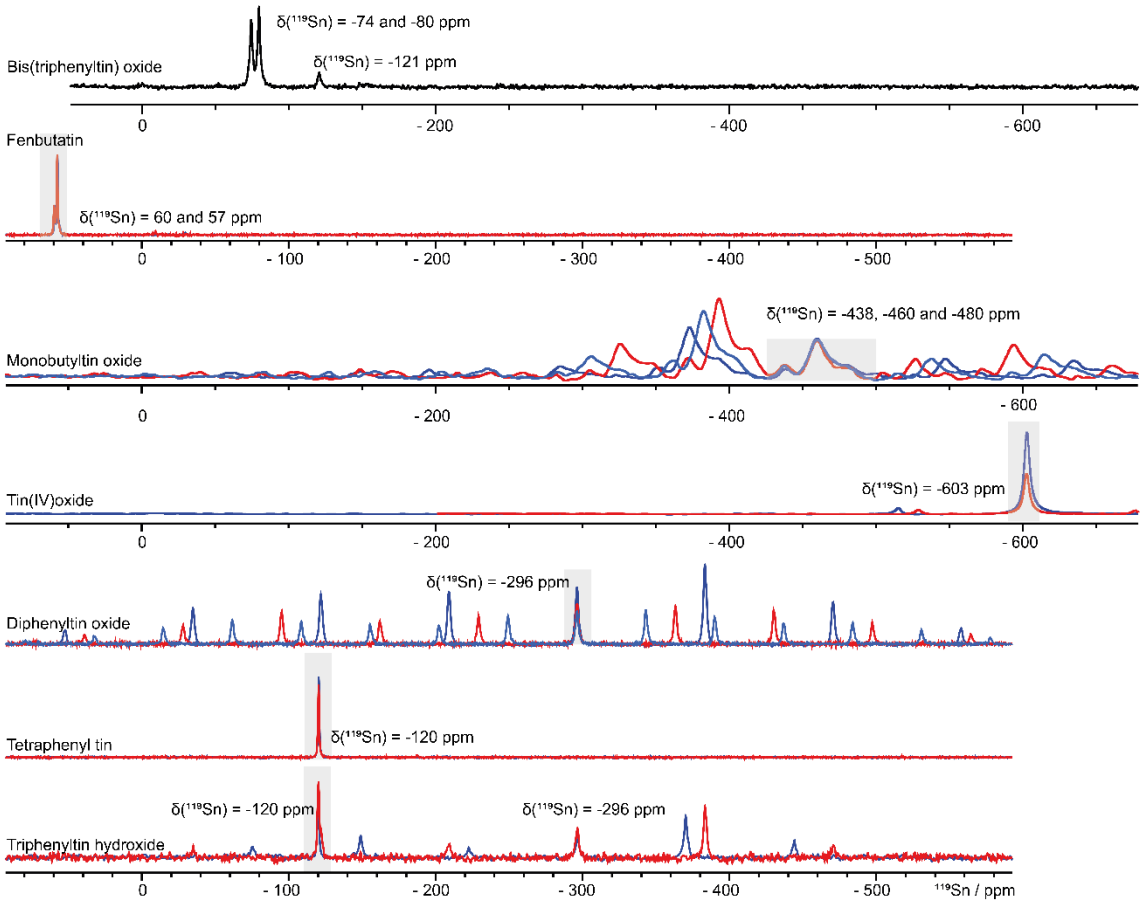

Figure 24. Summary of the ^{119}Sn CP and DE spectra of the model organotin substrates. ^{119}Sn CP spectra of triphenyltin hydroxide (2048 scans, d1 = 2 s recycle delay) , tetraphenyl tin (200 and 100 scans, d1 = 10 s), diphenyltin oxide (200 and 100 scans, d1 = 10 s), monobutyltin oxide (200 and 100 scans, d1 = 10 s) and fenbutatin (140 and 50 scans, d1 = 10 s), measured with spinning rates of 7 to 13 kHz to separate the signals from upcoming spinning side bands, Tin(IV) oxide was measured with direct excitation and 26 or 4 scans and d1 = 40 s. The signals are highlighted with grey boxes. Triphenyltin oxide shows two signals at δ(^{119}Sn) = -296 ppm and -120 ppm. Both signals can be assigned to the reference samples of tetraphenyl tin oxide and diphenyl tin oxide.

Table 5. Overview of model organotin compounds of the ^{119}Sn NMR shifts from compounds measured in the solid state and in NMR in solution from literature and experimentally determined ^{119}Sn shifts from solid state NMR experiments. The solvent has only a small impact on the chemical shift as long as the solvent does not interact with the tin compound.[38] [a]Impurity at δ(^{119}Sn) = -121 ppm also observed by Reams[39] when investigating Ph_3SnOH.

compound	^{119}Sn chemical shift literature	^{119}Sn chemical shift experimental data in the solid-state
Bu^n_4Sn	**(+)-12 ppm in solid-state[40]**	-
Bu^n_3SnPh	**-41.7 ppm solid-state[41]**	-
$Bu^n_2SnPh_2$	-65.9 ppm solid-state[41]	-
Ph_3SnBu^n	-101.5 ppm in C_6D_6 [42]	-
Ph_4Sn	**-128.1 ppm in $CDCl_3$ [43] -120.6 ppm solid-state [44] -123.89 in $CDCl_3$[45] -121.1 ppm[46] -127 ppm in $CDCl_3$ [47] -117 ppm solid-state [48]**	-120 ppm
Ph_3SnMe	-93 ppm CH_2Cl_2[49]	-
Ph_3SnEt	-98.6 ppm in C_6D_6 [42] -98 ppm in CCl_4 30% [50]	-
Ph_3SnBr	-60.01 in $CDCl_3$ (0.236M)[45]	-
Bu_3SnOBu^t	-60 ppm [51]	-
Bu_3SnOPh	-105 ppm [51]	-
Ph_3-Sn-Sn-Ph_3	**-143.6 in $CDCl_3$ [52] -144.2 in C_6D_6 [42]**	-
$(Ph_3Sn)_2O$	**-80.6 ppm solid state [43] -85.5 ppm in $CDCl_3$ 5% [53]**	-74.5 ppm -79.8 ppm -121 ppm
SnO_2	**-604.3 ppm solid-state [54]**	
Ph_3SnOH	-87.1 ppm in CD_2Cl_2[55] (+)-86.0 ppm in $CDCl_3$ [56] 298 ppm solid-state[39]	(-120 ppm)[a] -296 ppm
$Ph_2Sn{=}O$	No data in literature found	-296 ppm
BuSnO(OH)	-439, -461, -479 [57]	-438 ppm -460 ppm -480 ppm
Ph_2SnCl_2	-26.4 ppm[47]	-29.7 ppm

References

1. A. R. a. Consulting., Rare Sugar Market (By Product: D-Mannose, Allulose, Tagatose, D-Xylose, L-Arabinose, L-Fucose, D-Psicose; By Application: Dietary Supplements, Cosmetics, Personal Care, Pharmaceuticals, Food and Beverages, Sweetner, Others) - Global Industry Analysis, Market Size, Opportunities and Forecast, 2019 - 2026, https://www.acumenresearchandconsulting.com/rare-sugar-market).
2. M. M. RESEARCH, Rare Sugar Market: Global Industry Analysis and Forecast (2023-2029), https://www.maximizemarketresearch.com/market-report/rare-sugar-market/146022/).
3. I. Delidovich and R. Palkovits, *ChemSusChem*, 2016, **9**, 547-561.
4. I. Delidovich, P. J. Hausoul, L. Deng, R. Pfützenreuter, M. Rose and R. Palkovits, *Chemical reviews*, 2016, **116**, 1540-1599.
5. L. T. Mika, E. Cséfalvay and Á. Németh, *Chemical reviews*, 2018, **118**, 505-613.
6. H. van BEKKUM and A. C. Besemer, *Khimiya v Interesach Ustoichivogo Razvitiya*, 2003, **11**, 11-21.
7. D.-M. Gao, X. Zhang, H. Liu, H. Fujino, T. Lei, F. Sun, J. Zhu and T. Huhe, *Green Energy & Environment*, 2023.
8. S. Mahmood, M. W. Iqbal, W. Zhang and W. Mu, *Food Research International*, 2021, **145**, 110409.
9. K. Okano, *Tetrahedron*, 2009, **65**, 1937-1949.
10. H. Xiao, G. Wang, P. Wang and Y. Li, *Chinese Journal of Chemistry*, 2010, **28**, 1229-1232.
11. J. Huang, Z. Chen, W. Zhang, T. Zhang and W. Mu, *Applied microbiology and biotechnology*, 2018, **102**, 2051-2062.
12. N. A. Kocharova, O. G. Ovchinnikova, F. V. Toukach, A. Torzewska, A. S. Shashkov, Y. A. Knirel and A. Rozalski, *Carbohydrate research*, 2005, **340**, 1419-1423.
13. M. Moliner, Y. Román-Leshkov and M. E. Davis, *Proceedings of the National Academy of Sciences*, 2010, **107**, 6164-6168.
14. M. L. Hayes, N. J. Pennings, A. S. Serianni and R. Barker, *Journal of the American Chemical Society*, 1982, **104**, 6764-6769.
15. K. Izumori, *Naturwissenschaften*, 2002, **89**, 120-124.
16. N. Mijailovic, A. Nesler, M. Perazzolli, E. Aït Barka and A. Aziz, *Molecules*, 2021, **26**, 1720.
17. R. Stockman, J. Dekoninck, B. Sels and P. Jacobs, in *Studies in Surface Science and Catalysis*, Elsevier, 2005, vol. 156, pp. 843-850.
18. L. Petruš, M. Petrušová and Z. Hricovíniová, *Glycoscience: epimerisation, isomerisation and rearrangement reactions of carbohydrates*, 2001, 15-41.
19. V. Bilik, *Chem. zvesti*, 1972, **26**, 372-375.
20. M. Rellán-Piñeiro, M. Garcia-Ratés and N. López, *Green chemistry*, 2017, **19**, 5932-5939.
21. F. Ju, D. VanderVelde and E. Nikolla, *Acs Catalysis*, 2014, **4**, 1358-1364.
22. W. R. Gunther, Y. Wang, Y. Ji, V. K. Michaelis, S. T. Hunt, R. G. Griffin and Y. Roman-Leshkov, *Nature communications*, 2012, **3**, 1109.
23. I. Delidovich, A. Hoffmann, A. Willms and M. Rose, *ACS Catalysis*, 2017, **7**, 3792-3798.
24. M. J. Duer, *Solid state NMR spectroscopy: principles and applications*, John Wiley & Sons, 2008.
25. B. Reif, S. E. Ashbrook, L. Emsley and M. Hong, *Nature Reviews Methods Primers*, 2021, **1**, 2.
26. H. Günther, *NMR spectroscopy: basic principles, concepts and applications in chemistry*, John Wiley & Sons, 2013.
27. R. W. Schurko and M. J. Jaroszewicz, *The Lightest Metals, Encyclopedia of Inorganic and Bioinorganic Chemistry*, 2015, 117-172.
28. L. Qi, R. Alamillo, W. A. Elliott, A. Andersen, D. W. Hoyt, E. D. Walter, K. S. Han, N. M. Washton, R. M. Rioux and J. A. Dumesic, *ACS Catalysis*, 2017, **7**, 3489-3500.

29. E. D. Walter, L. Qi, A. Chamas, H. S. Mehta, J. A. Sears, S. L. Scott and D. W. Hoyt, *The Journal of Physical Chemistry C*, 2018, **122**, 8209-8215.
30. C. Sievers, Y. Noda, L. Qi, E. M. Albuquerque, R. M. Rioux and S. L. Scott, *ACS Catalysis*, 2016, **6**, 8286-8307.
31. V. Toussaint, I. Delidovich, S. Bachmann and A.-C. Pöppler, 2023.
32. T. Allscher, P. Klüfers and P. Mayer, *Glycoscience; Springer: Berlin/Heidelberg, Germany*, 2008, 1077.
33. J. Kragten, *Talanta*, 1975, **22**, 505-510.
34. R. Bermejo-Deval, R. Gounder and M. E. Davis, *ACS catalysis*, 2012, **2**, 2705-2713.
35. C. Li, Y. Wang, Y. Zhang, M. Wang, X. Sun, H. Cui and Y. Xie, *ChemistrySelect*, 2020, **5**, 270-279.
36. A. Cybulski, B. Kuster and G. Marin, *Journal of molecular catalysis*, 1991, **68**, 87-103.
37. S. Rojas-Buzo, A. Corma, M. Boronat and M. Moliner, *ACS Sustainable Chemistry & Engineering*, 2020, **8**, 16143-16155.
38. A. G. Davies, *Organotin Chemistry, Second Edition* Wiley-VCH Verlag GmbH & Co. KGaA., 2004.
39. P. W. Reams, Durham University, 1986.
40. J. J. Burke and P. C. Lauterbur, *J Am Chem Soc*, 2002, **83**, 326-331.
41. B. K. Hunter and L. W. Reeves, *Can J Chem*, 1968, **46**, 1399-1414.
42. M. Gielen, *Bulletin des Sociétés Chimiques Belges*, 1983, **92**, 409-410.
43. J. Holeček, M. Nádvorník, K. Handlíř and A. Lyčka, *J Organomet Chem*, 1983, **241**, 177-184.
44. R. Jamieson, PhD, The University of Guelph, 2013.
45. I. Wharf, *Inorg Chim Acta*, 1989, **159**, 41-48.
46. M. Charissé, A. Zickgraf, H. Stenger, E. Bräu, C. Desmarquet, M. Dräger, S. Gerstmann, D. Dakternieks and J. Hook, *Polyhedron*, 1998, **17**, 4497-4506.
47. C. Zeppek, J. Pichler, A. Torvisco, M. Flock and F. Uhlig, *J Organomet Chem*, 2013, **740**, 41-49.
48. R. A. Komoroski, R. G. Parker, A. M. Mazany and T. A. Early, *J. Magn. Reson. (1969-1992)*, 1987, **73**, 389-398.
49. A. G. Davies, P. G. Harrison, J. D. Kennedy, T. N. Mitchell, R. J. Puddephatt and W. McFarlane, *J. Chem. Soc. C*, 1969, DOI: 10.1039/j39690001136.
50. W. McFarlane, J. C. Maire and M. Delmas, *J Chem Soc, Dalton Trans*, 1972, DOI: 10.1039/dt9720001862.
51. P. J. Smith, R. F. M. White and L. Smith, *J Organomet Chem*, 1972, **40**, 341-353.
52. T. N. Mitchell and G. Walter, *J Chem Soc, Perkin Trans 2*, 1977, DOI: 10.1039/p29770001842.
53. S. Kerschl, B. Wrackmeyer, D. Männig, H. Nöth and R. Staudigl, *Z. Naturforsch. B*, 1987, **42**, 387-394.
54. N. J. Clayden, C. M. Dobson and A. Fern, *J Chem Soc, Dalton Trans*, 1989, DOI: 10.1039/dt9890000843.
55. F. Fresno, D. Tudela, A. J. Maira, F. Rivera, J. M. Coronado and J. Soria, *Appl Organomet Chem*, 2006, **20**, 220-225.
56. W. McFarlane and R. J. Wood, *J Organomet Chem*, 1972, **40**, C17-C20.
57. F. Ribot, C. Eychenne-Baron, F. Fayon, D. Massiot and B. Bresson, *Main Group Met Chem*, 2002, **25**.